

Dielectric EM Field Probes for HPM Test & Evaluation

Richard Forber*, W.C. Wang, and De-Yu Zang
IPITEK, 2330 Faraday Ave., Carlsbad, CA 92008.

Stephen Schultz and Richard Selfridge
Dept. of Electrical & Computer Engineering,
Brigham Young University, Provo, UT 84602

ABSTRACT

To meet test and evaluation needs for high power microwave (HPM), we describe developments on miniature all-dielectric optical E-field sensors with flat RF sensing response from ~MHz to 12 GHz, with negligible field perturbation, good sensitivity (~2V/m), and >100dB dynamic range. Initial devices use a 20 mm long sensing region in an integrated optical (IO) waveguide Mach-Zehnder interferometer (MZI) using electrooptic (EO) polymer for the optical waveguide. The fiber-coupled optical transmitter/receiver utilizes common photonic communication technology that enables sensor remoting with negligible RF loss. The incident HPM RF field induces an instantaneous change in the index of refractive of the polymer that is converted into an optical intensity modulation in the sensor device. The poled EO polymer requires neither electrodes nor metallic antennas that can distort the field under test. We characterized the frequency response and polarization sensitivity of the field sensor, with good agreement to modeling predictions. We also developed paths for extending bandwidth and for coupling multiple sensors into arrays. Sensor bias stabilization is developed to eliminate sensitivity to thermal drift and enable self-calibration. To further reduce the sensor size and insertion loss, beneficial for array applications, an “in-fiber” field sensor is also under development. The core of a D-shaped fiber is partially removed and replaced with EO polymer. Such a device could detect the RF field either by polarimetric sensing, by use of MZI structures as for the IO waveguide sensors.

1. INTRODUCTION

Aimed at test and evaluation (T&E) needs on high power microwave (HPM) weapons, the E-fields probes must minimally perturb the fields they are measuring, must not have a perceptible effect on monitored electronics, and must meet certain size specifications. To meet these measurement requirements for T&E, we are developing ultra wideband, all-dielectric, field probes based on novel EO polymer devices, including integrated optic waveguide devices and new “in-fiber” devices. The major advantages of our techniques include: a) extremely high bandwidth (to 100 GHz); b) very high spatial resolution (mm dimension);

c) minimum field invasiveness (< 5 % perturbation) because of low dielectric loss and absence of metallic electrodes; and, (d) very high damage threshold (> 700kV/m).

An integrated optic waveguide MZI E-field sensor was described in our previous work,^{1,2} where the sensor was tested at RF frequency up to 1 GHz. Here we utilize a tightly shielded fiber-coupled optical transmitter/receiver, and we report on measurements at higher RF frequency (to 12GHz) as well as sensitivity to RF polarization. Previously reported integrated MZI E-field sensors are susceptible to bias drift (sensitivity variation) from thermal and stress effects, and are not readily stabilized. We present revised sensor schemes that incorporate automated phase control and can be self-calibrated. To achieve the smallest sensor size for tightly confined environments, we are developing more miniaturized sensors and even “in-fiber” devices. The latter are produced in the core of a D-shaped fiber by partially removing core material and replacing it with EO polymer. Small and low-loss sensors are being developed for sensor arrays that will enable comprehensive HPM field mapping and characterization.

2. MZI E-FIELD PROBE

2.1 OPERATION THEORY

In the base configuration of a polymer MZI modulator, the EO active arms of the interferometer are oppositely poled (see Fig. 1b) utilizing metallic electrodes. Later, the poling electrodes are removed and the polymer waveguide layer is sandwiched into an all-dielectric packaging (see Fig. 1c). An external electric field uniformly applied to the two MZI sensor arms causes a relative phase difference between the optical waves in the two arms, resulting in modulated optical output intensity.

The phase retardation in the MZI EO polymer section of length L is given by

$$\phi = \pi n^3 r_{\text{eff}} E L / \lambda \quad (1)$$

where n is the index of refraction, r_{eff} is the effective EO coefficient, E is the applied external E-field, and λ is the laser wavelength. This phase change results in an output intensity change when the two beams are recombined interferometrically. The MZI output intensity I_o , modulated by the phase difference between the two arms can be expressed as:

$$I_o(E) = k I_i \cos^2[(\Delta\phi_{21} + \Delta\phi_{21}(E))/2] \quad (2)$$

where $\Delta\phi_{21} = \phi_2 - \phi_1$ is the built-in phase difference related to device fabrication factors, $\Delta\phi_{21}(E) = \Delta\phi_2(E) - \Delta\phi_1(E)$ is the phase difference induced by external electric field E, k is an attenuation factor due to insertion loss, and I_i is the input intensity.

* rforber@ipitek.com, 760-438-1010 x 3638 (phone), 760-438-2412 (fax)

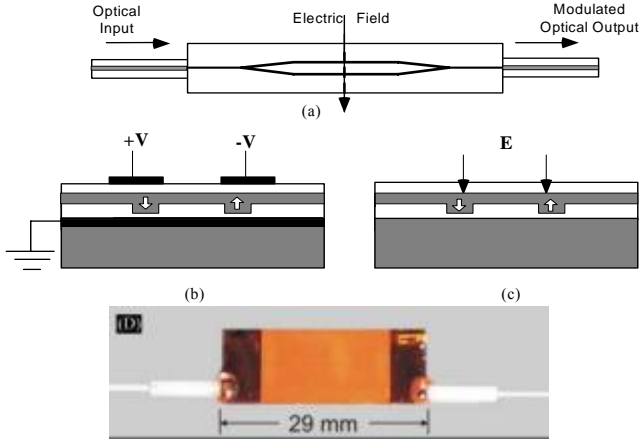


Fig. 1. A schematic design of the all-dielectric polymer waveguide E-field sensor. The polymer waveguides are poled utilizing electrodes as in (b). The poling electrodes are removed (c) leaving an all-dielectric device. When the sensor is subjected to an oscillating external field, an equal and opposite phase is built up between the MZI arms, leading to intensity modulation at the MZI output. (d) A picture of all-dielectric MZI field sensor.

A commonly used figure of merit is the electric field that corresponds to a phase shift of π in Eq. (2) and which is defined as:

$$E_{\pi} = \lambda / (n^3 r_{\text{eff}} L) \quad (3)$$

For the LD-3 polymer currently used in our device, and assuming efficient poling to achieve r_{eff} close to the r_{33} value of 5-8pm/V, the nominal value of E_{π} is 2-3 MV/m. By implementing a push-pull poling scheme³ (see Fig. 1b), the electro-optic effect in the two arms will align in opposite directions as shown in Fig. 1c, and the combined field-induced phase shift is doubled, reducing E_{π} by half since the shift in both arms of the interferometer will be equal and opposite. The optical output intensity in Eq. (2) can thus be rewritten as

$$I_o(E) = kI_i [1 + \cos(\Delta\phi_{21} + \pi E/E_{\pi})] / 2 \quad (4)$$

This equation simplifies further when the “built-in” phase difference $\Delta\phi_{21}$ is equal to $\pi/2$, which is the optimum bias point, commonly called the *quadrature operating point*. In that case,

$$I_o(E) = kI_i [1 - \sin(\pi E/E_{\pi})] / 2 \quad (5)$$

and the E-field modulation is maximized. For values of $E/E_{\pi} \ll 1$ (i.e. E is much smaller than 1 MV/m), the output intensity modulation is linear with the input RF E-field modulation,

$$I_o(E)|_{\text{mod}} = (\pi k / 2) [E/E_{\pi}] I_i \quad (6)$$

and negligible spurious harmonics are generated *as long as* the bias point of the MZI remains within the 1dB compression points ($\pm 0.36\pi/2$ from the *quadrature point*), as shown in Fig. 2. This is an important point since it means that MZI bias control is relatively relaxed for typically small detected E-field strengths ($\ll 2$ MV/m).

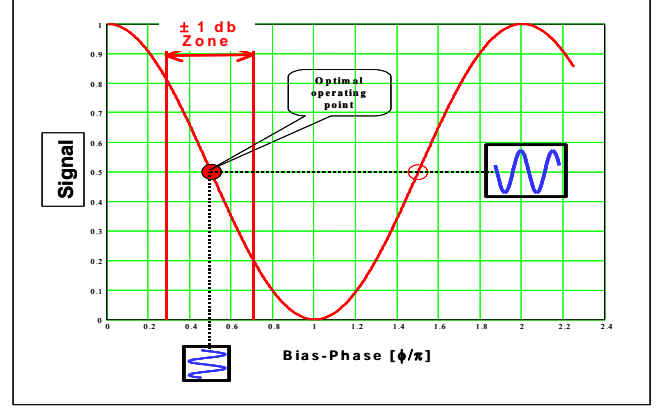


Fig. 2. Calculated sensor sinusoidal output intensity showing optimum phase bias at $\pi/2$, in the center of the linear response zone. For small modulation, and for phase bias within the 1 dB compression points, the sensor linearly translates input RF modulation to output signal.

Assuming the applied E-field is an oscillating RF signal⁽³⁾ at Ω , the E-field sensor optical signal oscillates in direct proportion to the RF field:

$$I_o(\Omega)|_{\text{mod}} = (\pi k / 2) [E(\Omega)/E_{\pi}] I_i \quad (7)$$

This RF modulated lightwave returns via a SM fiber to the receiver electronics (see Fig. 3), where it produces photocurrent in a high-speed photodetector. The RF photocurrent is amplified by a low noise amplifier (LNA), which provides the output of the sensor transceiver electronics. Typically, this output is input to a spectrum analyzer with a 50 Ω nominal input impedance. The electrical RF power measured by the spectrum analyzer is quadratic with the sensed RF electric field and, thus, is linear with the RF field power.

2.2 DEVICE FABRICATION

The fabrication process of MZI polymer thin film EO devices (Fig. 1) is briefly described herein. A uniform gold layer was first evaporated on a glass substrate for use as a lower poling electrode. A lower polymer cladding of ~ 4 μm thick thermoset polyurethane was spun on and cured at 120 C. The waveguide channels were defined photolithographically and were etched into the cladding layer by using oxygen plasma reactive ion etching. A thermally crosslinkable polymer containing amino-sulfone substituted azo dye (LD-3) was then spin-coated on the patterned lower cladding layer with a thickness of ~ 2 μm .

The polymer was then covered by thermoset polyurethane and UV light curable epoxy (Norland 73) as its top cladding layer with thickness of $\sim 4 \mu\text{m}$. After drying and curing, the top poling electrodes were deposited and lithographically patterned. The polymer was then heated to $\sim 130 \text{ C}$, poled under an intense electric field ($\sim 100 \text{ V}/\mu\text{m}$), and then cooled back to room temp. The polymer poling remains intact up to temperatures well below the glass transition temperature, and can be made more stable by polymer cross-linking. For cross-linked LD-3, for example, the device can withstand up to $\sim 140 \text{ C}$. The top poling electrode (as shown on Fig. 1b) was removed by standard wet-etching and the polymer EO device was then peeled off using a dry lift-off technique.⁴ The device was sandwiched between two fused silica slides for protection and to facilitate fiber pigtailing. Polarization maintaining (PM) and single mode (SM) fibers were pigtailed to the device for optical input and output coupling, respectively. The total device substrate was 3 cm long while the MZI “sensor” arms were 2 cm long. A picture of the pigtailed sensor is shown in Figure 1(d).

2.3 TEST DATA

The sensor testing setup is schematically shown in Fig. 3. The sensor head is linked to an optical transceiver by a pair of 20 meter long polarization maintained (PM) and single mode (SM) fibers. The optical transceiver (see Fig. 3) is composed of a CW laser (1310 nm DFB single mode laser with power of 30 mW), coupled to the PM fiber via a polarization controller and a linear polarizer. The receiving side includes a wideband photoreceiver (Discovery Semiconductors, Inc. R402 with BW of 10 GHz) coupled with a low noise RF amplifier (Cernex 40 dB gain with BW of 10 GHz).

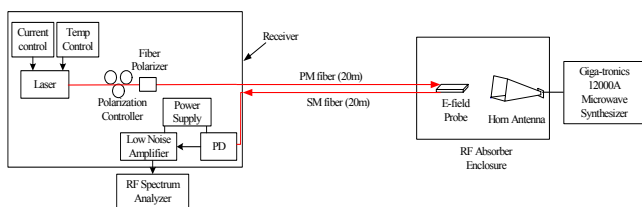


Fig. 3. Setup for testing E-field probe, where the sensor is enclosed by RF absorber and is linked to an optical transceiver by a pair of long PM and SM fibers. The optical transceiver is mounted in metallic box and it is composed of a laser source, a photoreceiver and low noise amplifier, a polarizer and a polarization controller and various accessories.

The transceiver was enclosed in a shielded metallic box. During the tests, the sensor head was located within a uniform E-field inside an RF absorber enclosure. In most of the cases, the sensor was aligned with its poling axis parallel to the linearly polarized E-field. In this alignment, the maximum signal is expected. The RF E-field was radiated by a set of horn antennas covering the high frequency (2.6 – 12 GHz) band. Higher frequencies ($>12\text{GHz}$) could not be directly tested due to BW limitations of the photoreceiver

and the LNA. Elimination of RF pick-up by elements such as the laser and the photoreceiver was ensured by the transceiver and RF source shielding, and tens of meters separation between the two.

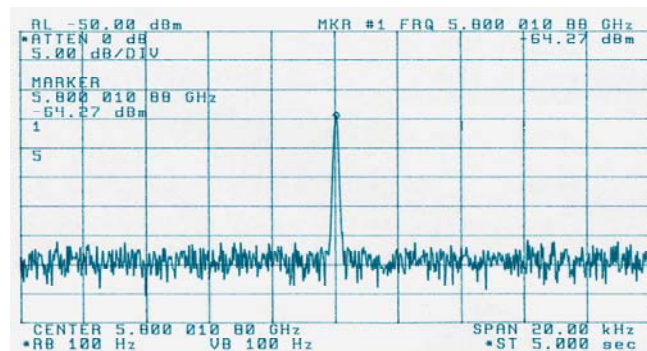


Fig. 4. A typical RF spectrum detected by a MZI field sensor, where the RF frequency is at 5.8 GHz and its E-field strength is about 76 V/m.

A typical spectrum of detected RF at 5.8 GHz is shown in Fig. 4, where the RF, with a E-field strength of about 76 V/m, propagates parallel with optical probe. The sensitivity of the field sensor can be determined from the data of the RF power dependence, which is about $70 \text{ mV}/(\text{m}\sqrt{\text{Hz}})$.⁵ The on-axis horn antenna field strength was estimated using the basic antenna equation⁶. The power density P_D , in the far field zone can be expressed by $P_D = P_{in}G\eta/(4\pi R^2)$, where P_{in} is the power input to the antenna, R is the distance from the antenna, G is the horn antenna gain, and $\eta \sim 0.7$ is the typical aperture efficiency of a rectangular horn antenna. The free space power density is translated into field strength by $P_D = E^2/Z$, where $Z=377 \Omega$ is the characteristic impedance of free space.

In Fig. 5 we show the sensitivity dependence on RF frequency by combined frequency response data obtained with four horn antennas. The field strength at the sensor location was normalized from one horn radiator to the next, producing a smooth transition in data from the separate horns. The all-dielectric sensor was tested with the RF wave propagating parallel and anti-parallel with the MZI optical probe. Due to transit time effects⁷ the parallel case shows a broader bandwidth. A theoretical calculation of the expected response for both RF propagation directions relative to the all-dielectric sensor axis is displayed by the continuous lines in Fig. 5. The calculation is based on a 20 mm long EO section, with optical refraction index of 1.6. The refraction index associated with the propagating RF field is assumed to be 1 due to the very shallow penetration [in wavelength units] of the RF wave into the optical waveguide structure. Note that the experimental data is normalized to the frequency response of the 10 GHz 3dB bandwidth photoreceiver. The sensitivity spectral results fit well the theoretical prediction. We note that for perpendicular RF incidence (plane orthogonal to the MZI axis, not plotted in Fig. 5), the response falls between the two curves shown.

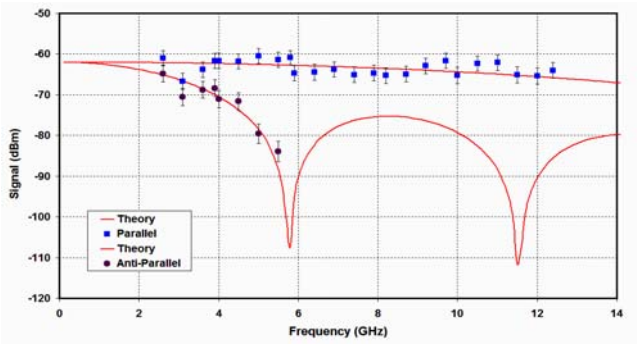


Fig. 5. Frequency response measurement of the all-dielectric field sensor, where the RF wave propagation direction is either parallel or anti-parallel with the light probe. The E-field was normalized to 76.2 V/m. The solid lines are the calculated response based on transit time considerations. The signal versus frequency is corrected for the photodiode response that drops off at 10 GHz. Note that the LNA is not a bandwidth-limiting component up to 20 GHz.

The data shown in Figs. 4 and 5 are measured when the E-field polarization is parallel to the poling axis of EO polymer. Due to the anisotropy of the poled polymer, the EO sensor is sensitive to the E-field polarization. The EO-induced index change by an RF E-field is proportional to the projection of the E-field vector on the polymer poling axis. Therefore, the sensor signal, that is linear with the EO index change, is proportional to $\cos(\alpha)$, where the angle α is between the E-field and the polymer poling axis. To verify that, the field sensor was mounted on a rotation stand and the angle dependence of the RF signal was measured and plotted in Fig. 6. As is expected, the signal on the spectrum analyzer, which is proportional to the square of the photocurrent on photo detector, is proportional to $\cos^2(\alpha)$. From the data we conclude the sensor can detect the RF polarization angle to within better than ± 2 degrees. For passive angle detection (non-rotatable sensor) two or three sensors in close proximity will be needed.

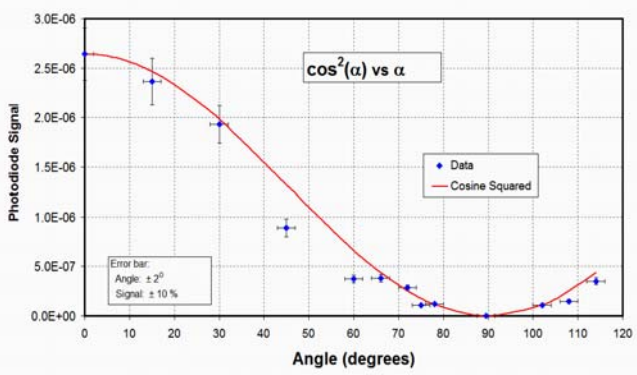


Fig. 6. Polarization dependence of the detected RF signal, where the RF propagate in parallel direction with optical probe.

2.4 BIAS CONTROL

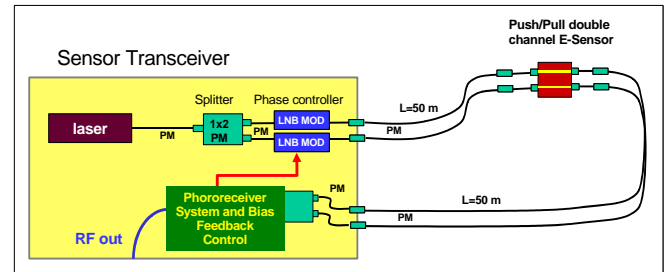


Fig. 7. The schematic of a proposed bias-stabilized E-field sensor. Phase drift in the fiber-based MZI is compensated by active control of the phase modulators in the transceiver. The use of two modulators reduces the asymmetry of the two arms.

With the integrated MZI sensor, we observed that the detected RF signal is not stable and undergoes slow cycling (temperature and/or stress related). As can be seen from Fig. 2, the bias point of the MZI will affect the detected RF signal level. The bias point shift will lead to an appreciable signal distortion if the bias point is outside the 1 dB compression range. The origin of the bias drift is due to slightly different temperature phase coefficients of the two MZI arms. The temperature affects the effective optical path length through both length and index variations. Since on-chip active bias and/or temperature control involves metallic components in the sensor head, we rather pursue a remote phase control in an extended MZI, as shown in Fig. 7.

The extended MZI arms contain a pair of single channel E-sensor devices as well as a pair of phase modulators (for balance). The total length mismatch between the two extended MZI arms is less than 10 mm, and path-dependent loss is also well matched (< 1 dB). Such a sensor with 20 m of PM fiber for remoting is shown in Fig. 8.

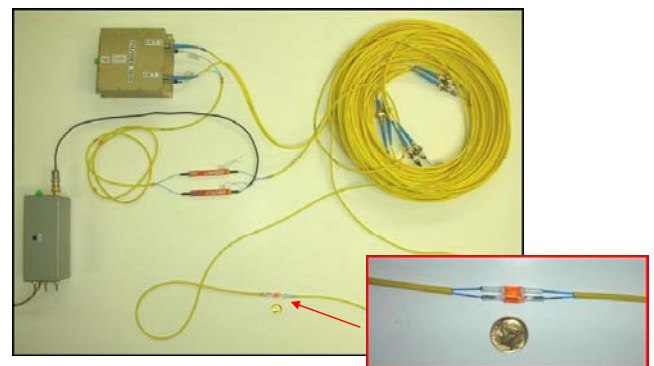


Fig. 8. Layout and detail of a bias-stabilized E-field sensor.

A simple COTS modulator bias controller (MBC) was able to lock the phase to the + (or -) quadrature bias point, as shown in Fig. 9. This encouraging initial result has large pilot tone amplitude and relatively slow locking response, however both are being addressed as we refine the approach.

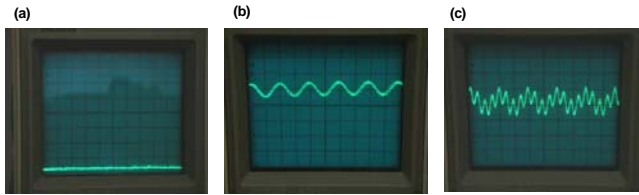


Fig. 9. Optical output of the extended MZI, where (a) MBC is off and bias is near null; (b) MBC is on but not locked yet and the bias is above quadrature; (c) MBC is locked and the bias is near quadrature.

A typical RF signal detected by this extended MZI field sensor is shown in Fig. 10.

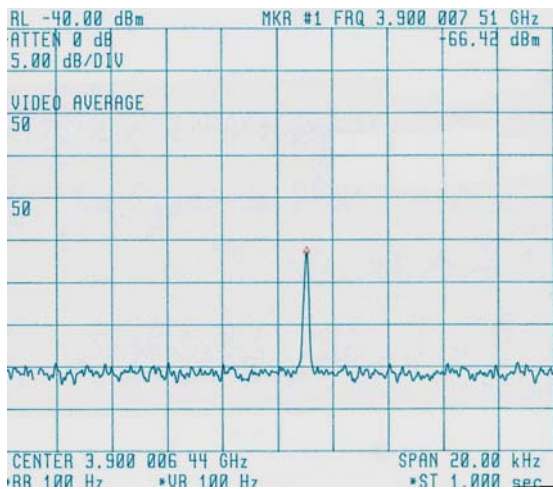


Fig. 10. A typical RF signal at 3.9 GHz that was detected by the extended MZI field sensor with MBC.

3. D-FIBER E-FIELD SENSOR

As shown in Fig. 7, the sensor is connected to standard optical fiber equipment, necessitating the connection between optical fiber and the integrated optical waveguides. In general, such a connection between the optical fiber and integrated optical waveguides requires active alignment (costly) as well as specific fabrication techniques to match the optical mode for low loss. Therefore, we are also developing an “in-fiber” sensor that requires no pigtailed and can have very low optical loss. In this “in-fiber” sensor a section of the core of an optical fiber is replaced with the EO polymer. The result of this core replacement technology is that the light remains within the optical fiber environment, thus eliminating the active alignment and packaging between the optical fiber integrated waveguide.

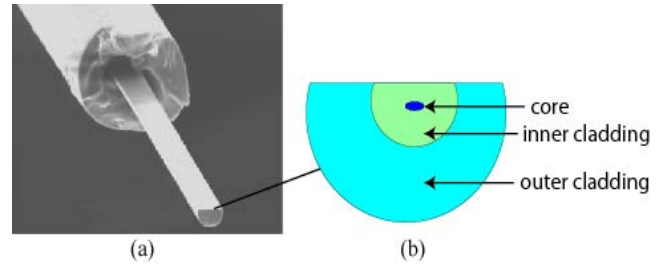


Fig.11. (a) Scanning electron microscope (SEM) image of a D-fiber with (b) a cross-sectional illustration of the optical fiber. The D-fiber consists of an elliptically shaped germanium-doped core, a fluorine-doped inner cladding, and an undoped outer cladding, where the distance between the core and the flat surface is around 12 μm .

This core replacement technology is attained by using D-fiber produced by KVH Industries. Figure 11 shows that the D-fiber has a cladding cross-section shaped like a “D”. This cladding shape places the core close to the flat side of the optical fiber. A section of the fiber is placed in hydrofluoric (HF) acid to remove a portion of the core of the D-fiber. The germanium-doped core etches around 8X faster than the surrounding cladding materials⁸. Figure 12 shows a cross-sectional SEM image of an etched optical fiber. The differential etch-rate results in a groove in the optical fiber where the core material was located.

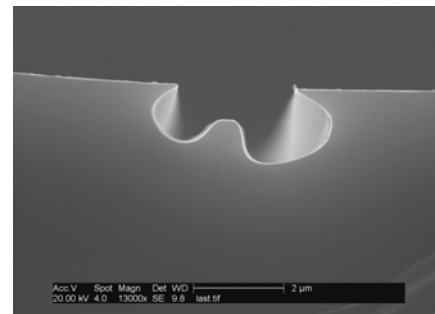


Fig. 12. SEM cross-sectional image of the region near the core of an etched D-fiber.

The EO polymer can then be spun into the groove. Figure 13 shows an SEM image of an etched fiber that has been coated with EO polymer. The core-replaced section of optical fiber can then be made sensitive to the incident RF field by poling the EO polymer, similar to what was done for the integrated optic waveguide devices described above. Various poling techniques are being developed, tested and evaluated.

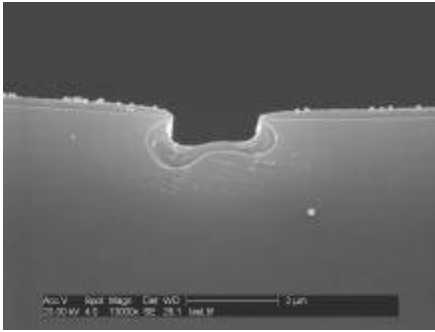


Fig. 13. SEM cross-section image of D-fiber in which EO polymer has been spun into the groove produced through etching in HF acid.

A successful D-fiber sensor implementation is expected to be an attractive ultra-miniaturized and low-loss sensing element for use in the bias-stabilized sensor scheme of Fig. 7, especially for sensor array applications. We envision the potential to embed such sensors into electronic circuits under test, as shown in Fig. 14.

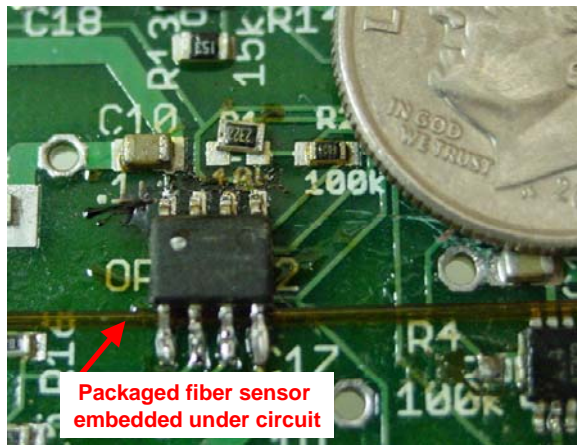


Fig. 14. Packaged D-fiber sensor embedded under electronic circuit elements.

4. CONCLUSION

An all-dielectric EO polymer MZI device (3cm x 1.2 cm) was demonstrated with sensitivity to free-space E-field RF signals over a wide frequency range from 200 MHz to 12 GHz. Both the frequency response and the RF field polarization dependence agree well with modeling prediction. With a detection limit of about 70 mV/(m $\sqrt{\text{Hz}}$) for a 2cm long all-dielectric MZI field sensor, this minimally perturbing sensor is well-suited to HPM effects characterization. A bias-stabilized sensor using an extended MZI scheme was developed and demonstrated. To further reduce the sensor size and insertion loss, both a single channel integrated optic waveguide device and an “in-fiber” device are being developed. Arrays of these miniaturized E-field sensors will allow detailed non-perturbing monitoring and characterization of HPM effects.

ACKNOWLEDGEMENT

The authors would like to thank the Test Resource Management Center Test & Evaluation/Science & Technology Program for their support. This work is funded through U.S. Army Program Executive Office for Simulation, Training & Instrumentation.

REFERENCES

- ¹ W.C. Wang, W. Lin, H. Marshall, D. Schaafsma, R. Chaung, “All-dielectric fiber-optic passive millimeter-wave antenna”, *SPIE*, **5100**, p.149-156, (2003).
- ² W.C. Wang, W. Lin, H. Marshall, R. Skolnick, D. Schaafsma, “All-dielectric miniature wide-band RF receive antenna”, *Optical Engineering*, **43**(3), p.673-677, (2004).
- ³ W. Wang, Y. Shi, D.J. Olson, W. Lin, and J.H. Bechtel, “Push-pull poled polymer Mach-Zehnder modulators with a single microstrip line electrode,” *IEEE Photon. Technol. Lett.*, 11, 51, 1999.
- ⁴ Y. Shi, A. Yacoubian, D.J. Olson, W. Lin, J.H. Bechtel, “Dry lift-off technology for Electrooptic polymer thin films and its photonic device applications”, *Proceedings of OSA Conference on Organic Thin Films*, Long Beach, CA, October 2001.
- ⁵ W.C. Wang, H. Lotem, R. Forber, and K. Bui, “Optical Electric-field sensors”, to be published in *Optical Engineering*, 2006.
- ⁶ D. Adamy, “*EW101: A first course in electronic warfare*”, Artech House, (2001).
- ⁷ Amnon Yariv, “*Quantum Electronics*”, John Wiley & Sons (1975), Chap. 14.
- ⁸ Douglas J. Markos, Benjamin L. Ipson, Kevin H. Smith, Stephen M. Schultz, Richard H. Selfridge, Thomas D. Monte, Richard B. Dyott, and Gregory Miller, “Controlled core removal from a D-shaped optical fiber,” *Appl. Opt.*, vol. 42, pp. 7121-7125, Dec. 2003.